Finite-size effects of avalanche dynamics

Christian W. Eurich*
Institut für Theoretische Physik, Universität Bremen, Otto-Hahn-Allee 1, D-28334 Bremen, Germany

J. Michael Herrmann
Max-Planck-Institut für Strömungsforschung, Bunsenstrasse 10, D-37073 Göttingen, Germany

Udo A. Ernst
Institut für Theoretische Physik, Universität Bremen, Otto-Hahn-Allee 1, D-28334 Bremen, Germany
(Received 14 September 2000; published 31 December 2002)

We study the avalanche dynamics of a system of globally coupled threshold elements receiving random input. The model belongs to the same universality class as the random-neighbor version of the Olami-Feder-Christensen stick-slip model. A closed expression for avalanche size distributions is derived for arbitrary system sizes N using geometrical arguments in the system's configuration space. For finite systems, approximate power-law behavior is obtained in the nonconservative regime, whereas for $N\to\infty$, critical behavior with an exponent of $-3/2$ is found in the conservative case only. We compare these results to the avalanche properties found in networks of integrate-and-fire neurons, and relate the different dynamical regimes to the emergence of synchronization with and without oscillatory components.

DOI: 10.1103/PhysRevE.66.066137 PACS number(s): 05.65.+b, 05.70.Ln, 45.70.Ht, 87.18.Sn

I. INTRODUCTION

In the last decade, a considerable number of publications have been dedicated to the occurrence of power-law behavior in systems involving interacting threshold elements driven by slow external input. The dynamics accounts for phenomena occurring in such diverse systems as piles of granular matter [1], earthquakes [2], the game of life [3], friction [4], and sound generated in the lung during breathing [5]. An avalanche of theoretical investigations was triggered by Bak, Tang, and Wiesenfeld [6] who linked the occurrence of power laws to the notion of self-organized criticality (SOC). In the so-called sandpile models, locally connected elements receiving random input self-organize into a critical state characterized by power-law distributions of avalanches without the explicit tuning of a model parameter (e.g., Refs. [7–18]). Analytical results were derived for sandpile models [14,15], and it was shown that the existence of a conservation law is a necessary prerequisite to obtain SOC [16–18].

A second class of models inspired by earthquake dynamics employs continuous driving and nonconservative interaction between the elements of the system [4,19]. In the Olami-Feder-Christensen (OFC) model [19], where the amount of dissipation is controlled by a parameter α, power-law behavior of avalanches occurs for a wide range of α values. Subsequent investigations emphasized the importance of boundary conditions and tied the existence of the observed scaling behavior to synchronization phenomena induced by spatial inhomogeneities [20–24]. More specifically, Lise and Jensen [25] introduced a random-neighbor interaction in the OFC model to avoid the buildup of spatial correlations. Further analysis indeed revealed that the random-neighbor OFC model does not display SOC in the dissipative regime [26–28].

In these avalanche models with nonconservative interaction, analytical results have been obtained only for system size $N\to\infty$ so far [26,29]. Here we introduce a model that not only circumvents the problem of system boundaries, but yields an analytical access also for finite system sizes N. The elements are globally connected, which makes the system a mean-field model. Randomness is not introduced through random neighbors but by providing a random external input. During an avalanche, the elements become unstable and relax in a fixed order determined by the state of the system immediately prior to the avalanche. Therefore, the system is strictly Abelian for dissipation parameters α smaller than a threshold value, which can be readily worked out. In this case, a geometrical approach in the N-dimensional configuration space yields an exact equation for the distribution of avalanche sizes.

In Sec. II, the model is specified and compared with other dissipative avalanche models, in particular, with the random-neighbor OFC model. In Sec. III, avalanche properties are presented both numerically and analytically, whereby details of the analytical calculation of the avalanche size distributions can be found in Appendixes A–C. Extensions and applications of the model are formulated in the terminology of neural networks: The model allows for an interpretation in terms of a fully connected neural network of nonleaky integrate-and-fire neurons. Implications of this view such as the synchronization behavior of local, densely connected populations of cortical neurons will be discussed in Sec. IV. The paper concludes with a brief summary and discussion.

II. THE AVALANCHE MODEL

A. Definition

In the model, time is measured in discrete steps, $t=0,1,2,\ldots$. Consider a set of N identical threshold ele-

*Electronic address: eurich@physik.uni-bremen.de

ments characterized by a state variable $u \geqslant 0$, which will henceforth be called *energy*. The system is initialized with arbitrary values $u_i \in [0,U)(i=1,\ldots,N)$, where U is the threshold above which elements become unstable and relax. Depending on the state of the system at time t, the ith element receives external input $I_i^{\mathrm{ext}}(t)$ or internal input $I_i^{\mathrm{int}}(t)$ from other elements, resulting in an activation $\tilde{u}$ at time $t+1$,

$$\tilde{u}_i(t+1) = u_i(t) + I_i^{\mathrm{ext}}(t) + I_i^{\mathrm{int}}(t). \tag{1}$$

From the activation $\tilde{u}_i(t+1)$, the energy of the ith element at time $t+1$ is computed as

$$u_i(t+1) = \begin{cases} \tilde{u}_i(t+1) & \text{if } \tilde{u}_i(t+1) < U, \\ \epsilon(\tilde{u}_i(t+1) - U) & \text{if } \tilde{u}_i(t+1) \geqslant U, \end{cases} \tag{2}$$

i.e., if the activation exceeds the threshold U, it is reset but retains a fraction $\epsilon (0 \leqslant \epsilon \leqslant 1)$ of the suprathreshold portion $\tilde{u}_i(t+1) - U$ of the energy.

For the external input $I_i^{\mathrm{ext}}(t)$, one element is randomly chosen from a uniform distribution at each time step, and a constant amount of energy $\Delta U \in (0,U]$ is added to the element's energy. The external input is considered to be delivered slowly compared to the internal relaxation dynamics, i.e., it occurs only if no element has exceeded the threshold in the previous time step. This corresponds to an infinite separation of the time scales of external driving and avalanche dynamics discussed in the SOC literature [11–13]. The external input can formally be written as $I_i^{\mathrm{ext}}(t) = \delta_{r(t),i}\delta_{M(t-1),0}\Delta U$. $r(t)$ is an integer random variable drawn at time step t from a uniform distribution between 1 and N, indicating the chosen element, $M(t-1)$ is the number of suprathreshold elements in the previous time step, and $\delta_{i,j}$ is the Kronecker delta.

The internal input $I_i^{\mathrm{int}}(t)$ is given by $I_i^{\mathrm{int}}(t) = M(t-1)\alpha U/N$, where $\alpha U/N$ is the coupling strength between the elements. We assume connections to be excitatory, that is, $\alpha > 0$.

At some time t_0 an avalanche starts, $M(t_0) = 1$, provided the element receiving external input becomes unstable. The system is globally coupled, such that during an avalanche all elements receive internal input, including the unstable elements themselves. The avalanche duration $D \geqslant 0$ is defined to be the smallest integer for which the stopping condition $M(t_0 + D) = 0$ is satisfied. The avalanche size L is given by $L = \sum_{k=0}^{D-1} M(t_0 + k)$. The model allows the calculation of the probability $P(L,N,\alpha)$ of an avalanche of size $L \geqslant 0$ in the regime $0 \leqslant L \leqslant N$ of a system consisting of N elements with coupling parameter α. Avalanche size distributions can alternatively be described by a function $p(L,N,\alpha)$ for $L \geqslant 1$, which is related to $P(L,N,\alpha)$ via

$$p(L,N,\alpha) \equiv \frac{P(L,N,\alpha)}{1 - P(0,N,\alpha)}. \tag{3}$$

Avalanche duration distributions will be denoted by $p_d(D,N,\alpha)(D \geqslant 1)$.

Due to the global coupling of the elements, there are no boundary conditions to be specified in the model.

B. The case $\epsilon = 1$

Both the coupling parameter α and the reset parameter ϵ control the amount of dissipation in the system. An analytical approach will be possible for $\epsilon = 1$, that is, if all suprathreshold elements are reset such that they lose an identical amount U of energy [cf. Eq. (2)]. We will therefore restrict further analysis to this case and only briefly return to the general situation in Sec. IV.

For $\epsilon = 1$, the value $\alpha = 1$ corresponds to the conservative case with respect to the internal dynamics: upon resetting of a suprathreshold element, the energy it loses is completely distributed in the network. For $\alpha \geqslant 1$, an infinite avalanche may eventually occur and we will therefore restrict ourselves to the case $\alpha < 1$. In order to avoid side effects resulting from the null set of rational values of α, U, or ΔU, we assume one of the fractions α/U or $\Delta U/U$ to be irrational. As will be shown below, a variation of α leads to qualitatively different avalanche size distributions.

C. Comparison with other avalanche models

A class of models discussed in the SOC literature employs a parameter controlling the amount of dissipation [4,19–28]. The numerically observed power-law behavior in such systems, however, could be ascribed to spatial inhomogeneities and the employed boundary conditions (e.g., [21–24]). In order to study avalanches of activity in the presence of dissipation independent of spatial correlations among elements, Lise and Jensen [25] introduced a random-neighbor version of the Olami-Feder-Christensen model described in Ref. [19]. In this model, threshold elements receive a constant, uniform input and have random nearest neighbors to which they are connected during an avalanche. The temporal variability of the network connectivity avoids the buildup of spatial correlations, thus ruling out boundary effects in shaping avalanche distributions. Subsequent studies, however, demonstrated that the random-neighbor OFC model does not have scaling behavior in the dissipative regime [26–28].

Bröker and Grassberger [26], in their analytical considerations of the random-neighbor OFC model, applied the theory of branching processes to yield avalanche size distributions. For this purpose it was necessary to consider the limits $d \to \infty$ (where d is the dimension of the lattice) and $N \to \infty$ in order to make the model effectively Abelian and avoid correlations among elements [26]. This prevents avalanches from visiting elements more than once and allows subavalanches to spread independently of each other such that each suprathreshold element has a distinctive predecessor which triggered it.

Our model poses an alternative of the random-neighbor OFC model: the global coupling of elements prevents spatial correlations and the putative dependence of the system behavior on boundary conditions. Randomness is introduced through the external input rather than the random assignment of nearest neighbors. This approach has the advantage of not requiring the limit $N \to \infty$: For $\epsilon = 1$, the system is Abelian

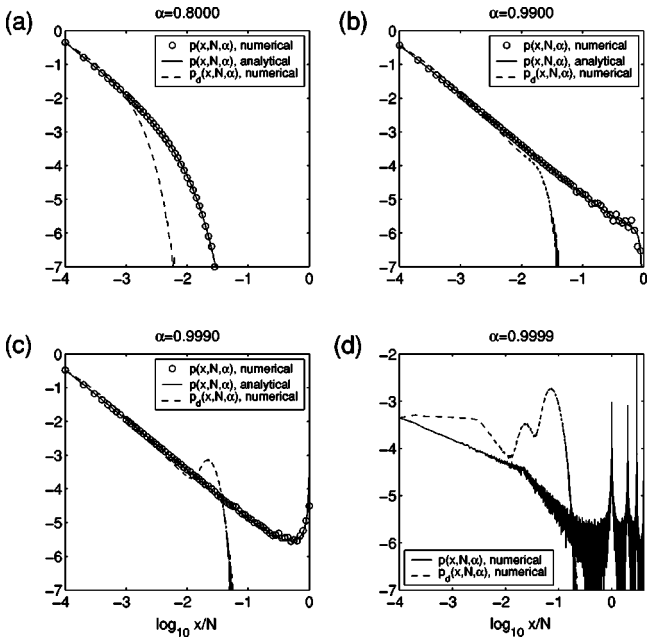

FIG. 1. Probability distributions of avalanche sizes, $p(x,N,\alpha)$, and avalanche durations, $p_d(x,N,\alpha)$, in the subcritical [(a), $\alpha=0.8$], critical [(b), $\alpha=0.99$], supracritical [(c), $\alpha=0.999$], and multipeaked [(d), $\alpha=0.999\,97$] regime. (a)–(c) Solid lines and symbols denote the analytical and the numerical results for the avalanche size distributions, respectively. In (d), the solid line shows the numerically calculated avalanche size distribution. The dashed lines in (a)–(d) show the numerically evaluated avalanche duration distributions. In all cases, the presented curves are temporal averages over 10^7 avalanches with $N=10\,000$, $\Delta U=0.022$, and $U=1$.

for an arbitrary system size N because at each time step t during an avalanche, all elements receive the same input depending only on the number $M(t-1)$ of suprathreshold elements at time $t-1$.

The random-neighbor OFC model and the globally coupled model are complementary in the following sense: in the random-neighbor OFC model, randomness is introduced through the random choice of neighbors during the avalanche activity, while the interavalanche dynamics is a simple shift of the energy distribution $\rho(u)$ on the u axis due to the uniform input. In our globally coupled model, the stochasticity is due to the random external input between avalanches, whereas the avalanche activity corresponds to a rotation of $\rho(u)$ on a circle $[0,U)$ with periodic boundary conditions. The latter property is due to (i) the fact that all elements—including the unstable ones—receive the same input $I_i^{\mathrm{int}}(t)$ at each time step, and (ii) the update rule (2) which reinjects unstable elements according to the suprathreshold portion $\tilde{u}_i(t+1)-U$ of their energy. Therefore, the elements become unstable in a fixed order depending on the actual distribution $\rho(u)$. Below it will be shown that for coupling coefficients $\alpha<\max\{1-\Delta U/U, N/(N+1)\}$, avalanche sizes may not exceed N, which means that each element can be activated only once. In this regime, avalanche distributions turn out to be very similar for the random-neighbor OFC model and the current model, demonstrating that the differences between the models barely change the statistical properties of the avalanches. However, in the globally coupled model, this regime can be described by a closed expression for avalanche distributions, $p(L,N,\alpha)$.

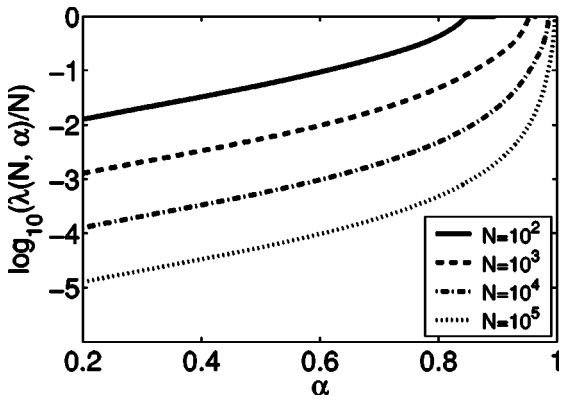

FIG. 2. Range $\lambda(N,\alpha)$ of avalanche sizes over which power-law behavior is observed in the subcritical regime. $\lambda(N,\alpha)$ has been plotted for four different system sizes, namely, for $N=10^2$ (solid line), $N=10^3$ (dashed line), $N=10^4$ (dashed-dotted line), and $N=10^5$ (dotted line). To obtain λ, $\hat{p}(L,N,\alpha)$ as defined in Eq. (4) has been fitted to the analytically calculated avalanche size distribution $p(L,N,\alpha)$ by maximizing the symmetric version of the Kullback-Leibler distance $K(\lambda)$ as defined by $K(\lambda)=\Sigma_L(p-\hat{p})[\ln(p)-\ln(\hat{p})]$.

III. AVALANCHE PROPERTIES

A. Avalanche sizes

Figure 1 shows avalanche size distributions for different values of α. $N=10\,000$ was chosen as the system size, but the curves look very similar for any other choice of N.

Four qualitatively different regimes can be distinguished which will be termed subcritical, critical, supracritical, and multipeaked. For small values of α, subcritical avalanche size distributions exist, which can be approximated by the general expression

$$p(L,N,\alpha)\approx\hat{p}(L,N,\alpha)=L^{\gamma}\exp(-L/\lambda), \tag{4}$$

where γ is an exponent independent of N to be characterized below, and $\lambda=\lambda(N,\alpha)$ describes the range of avalanche sizes over which power-law behavior is observed [Fig. 1(a)]. For fixed N, $\lambda(N,\alpha)$ is a monotonically increasing function of α as long as $\alpha<\alpha_c$ which we refer to as the "critical case" (Fig. 2). For α_c, the system has avalanche distributions with an approximate power-law behavior with exponent $-3/2$ from $L=1$ almost up to the size of the system, where the usual exponential cutoff is observed [49] [Fig. 1(b)]. For finite N, α_c is in the dissipative regime. Above the critical value α_c, avalanche size distributions become nonmonotonic [Fig. 1(c)]. Such supracritical curves have a minimum at some intermediate avalanche size.

In order to find the critical coupling coefficient α_c as a function of system size N, we computed a conveniently defined distance $K(\alpha)$ between the distribution $p(L,N,\alpha)$ and

an "ideal" power-law distribution $\tilde{p}(L,N)=L^{-3/2}/\Sigma_L L^{-3/2}$. Then $K(\alpha)$ was numerically minimized to yield the parameter α_c for which the distribution is closest to a power law. We chose the symmetric version of the Kullback-Leibler distance as defined by $K(\alpha)=\Sigma_L(p-\tilde{p})[\ln(p)-\ln(\tilde{p})]$, which revealed a critical coupling constant

$$\alpha_c(N)\approx 1-N^{-\mu} \quad \text{with} \quad \mu=0.5\pm 0.01 \tag{5}$$

(obtained for system sizes ranging from $N=10^2$ up to $N=10^7$). An alternative approach to obtain the exponent μ is to compute the slope of the avalanche size distribution $p(L,N,\alpha)$ for avalanche sizes $L=N/2$ using the analytical expression to be derived below. The result is $\mu=0.5$, in agreement with the numerics.

Above the supracritical case, a fourth regime exists for values of α close to 1, where the distributions show multiple peaks located at $L=N,2N+1,3N+1,\ldots$. These peaks arise from the high coupling strength because elements can become suprathreshold more than only once during an avalanche. This is not possible in the subcritical, critical, and supracritical regimes. Figure 1(d) shows an example with three peaks (note that the last maximum is not referred to as a peak).

Conditions for the occurrence of k peaks in the avalanche size distributions can be readily worked out. Consider the case $k=1$ corresponding to the situation that neurons may fire twice at most during an avalanche. First, an avalanche size $L=N+1$ must be possible. Since all elements receive the same internal input and fire in a fixed order as described above, this is equivalent to the condition that the element which originally triggered the avalanche may fire twice. After N firing events, this element has received the total input $\Delta U+\alpha U$. A second firing can thus occur if this input exceeds the threshold, or $\alpha>1-\Delta U/U$. Second, after $N+1$ firing events, the total internal input to each element must exceed the threshold to allow for further firing, $(N+1)\alpha U/N>U$ or $\alpha>N/(N+1)$. Similar arguments hold for the general case of k peaks. The above conditions must then be replaced by

$$\alpha>\alpha_{\min}(k)=\max\left\{1-\frac{\Delta U}{kU},\ \frac{kN}{kN+1}\right\}. \tag{6}$$

$\alpha_{\min}(k)<\alpha\leqslant\alpha_{\min}(k+1)$ then gives the range of coupling constants for which k peaks can be observed.

Examples for avalanche distributions in the multipeaked regime are shown in Fig. 3. The distribution functions between two peaks at $L=kN$ and $L=(k+1)N$ are always nonmonotonic. This can be seen as follows: In an avalanche of size larger than kN, the energies u_i must have been in an appropriate order to allow for this size. Because the interavalanche dynamics corresponds to a simple shift of $\rho(U)$ on the circle $(0,U)$, the ordering after kN events is nearly similar to the ordering prior to the start of the avalanche, except for the element which received external input. This element has been responsible for triggering the avalanche, and only this element has changed its position relative to the others. Therefore, it is highly probable that again all N elements will take part in the continuing avalanche, which explains the increase of the distribution towards $L=(k+1)N$. As can be seen from Fig. 3, all distributions have minima at avalanche sizes $L=N/2,3N/2,\ldots,(k+1/2)N,\ldots$.

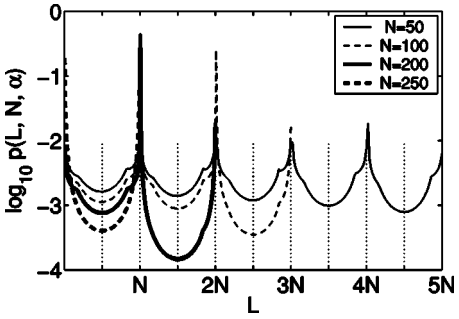

FIG. 3. Different avalanche size distributions $p(L,N,\alpha)$ with $\alpha=0.996$ for $N=50$ (thin solid line, four peaks), $N=100$ (thin dashed line, two peaks), $N=200$ (thick solid line, one peak), and $N=250$ (thick dashed line). The curves show maxima at $L=kN$ and minima at $L=(k+0.5)N$ (both marked with dotted lines). In all cases, the presented curves are temporal averages over 2×10^8 avalanches with $\Delta U=0.022$ and $U=1$.

B. Avalanche durations

In comparison to the avalanche size distributions described before, Fig. 1 also shows examples of avalanche *duration* distributions in the four different regimes. Qualitatively, the duration distributions have similar shapes. In the subcritical regime, the distributions are described by monotonically decreasing functions as in Eq. (4), and above the critical regime, the functions show one or more maxima as the coupling α increases, going from the supracritical to the multipeaked regime.

The critical case occurs for the same value α_c for which the size distribution is also critical [Fig. 1(b)], and the critical exponent is the same. This holds for all system sizes N we have tested (data not shown). That is, the dependence of the critical α on the system size N is given by the same expression (5) for the avalanche sizes and the avalanche durations.

The main difference to size distributions lies in the fact that duration distributions start to differ from an "ideal" power-law distribution at lower values of L. This behavior can be explained by an intuitive argument. For avalanche sizes of $L=N$, it is unimportant how many elements are triggered in each step of the avalanche as long as the total number of toppling elements is N. For an avalanche *duration* of N, it is not only required that the avalanche composed of N elements is being triggered, but it is also necessary that in each step of the avalanche, exactly *one* element is triggered. Hence large avalanche durations have a far lower probability than large avalanche sizes.

C. Analytical considerations

We use combinatorial arguments in the system's N-dimensional configuration space to derive expressions for avalanche size distributions in the subcritical, critical, and supracritical regimes. The configuration space $\Pi^N(0,U)$ (or simply Pi^N) is defined to be the Cartesian product

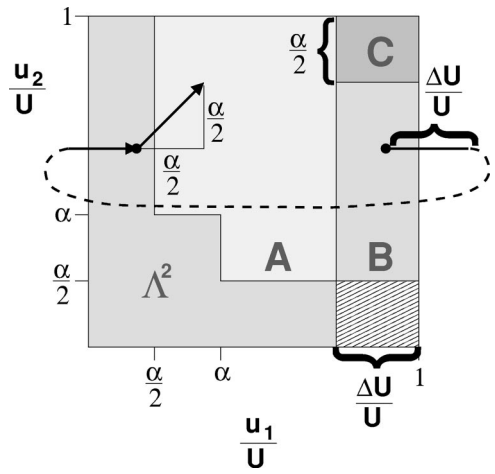

FIG. 4. The dynamics in the configuration space for $N=2$ elements. Effects of an external input to element 1 (line marked as $\Delta U/U$) followed by an avalanche of size 1 resulting in an input to both elements (arrow pointing along the diagonal). Λ^2 denotes the region where the density of states eventually vanishes; *A*, *B*, and *C* denote regions leading to avalanches of size $L=0,1,2$, respectively, if triggered by an external input to element 1. The hatched area leads to an avalanche of size 1 but lies within Λ^2.

$\Pi^N(0,U)=[0,U)^N$ with periodic boundary conditions, i.e., it has the topology of an *N*-torus (see Appendix A).

1. An example with two elements

The case $N=2$ demonstrates the basic mechanisms for evaluating the avalanche dynamics. The avalanche distribution is calculated by determining the equilibrium density of states in Π^2, $\rho(u_1,u_2)$, and subsequently considering the regions which lead to avalanches of sizes 0,1, and 2. Figure 4 shows the configuration space Π^2 and the shifts resulting from external input ΔU, internal input $\alpha U/2$, and avalanches of size $L=1$. In the latter case, the system leaves Π^2 and is reinjected on the opposite side. We consider $\rho(u_1,u_2)$ only at times between avalanches. Then, the total internal input distributed during an avalanche leads to a shift vector which guarantees that systems will never be reinjected into the region denoted by $\Lambda^2(\alpha,U)$, i.e., $\rho(u_1,u_2)=0$ for $(u_1,u_2)\in\Lambda^2$. The density in $\Pi^2\backslash\Lambda^2$ is solely determined by the randomly distributed external input. This input can be decomposed into deterministic shifts of size $\Delta U/\sqrt{2}$ along the diagonal $u_1=u_2$ and a random walk orthogonally to $u_1=u_2$. As a consequence of this stochasticity in combination with the reinjection after avalanches, the density in $\Pi^2\backslash\Lambda^2$ becomes constant for large times *t*, and a normalization yields the value $\rho(u_1,u_2)=[U^2(1-\alpha)]^{-1}$. Figure 4 also identifies those regions in Π^2 which lead to avalanches of sizes 0 (*B*), 1 (*C*), and 2 (*D*) following external input to element 1. Avalanche probabilities $P(L,2,\alpha)$ are obtained by integrating $\rho(u_1,u_2)$ over the respective region. Using Eq. (3), the result is

$$p(1,2,\alpha)=\frac{2(1-\alpha)}{2-\alpha} \quad \text{and} \quad p(2,2,\alpha)=\frac{\alpha}{2-\alpha}. \tag{7}$$

2. The general case of N elements

Similar arguments hold for the general situation of *N* elements. The topology of region Λ^N—the region which is not inhabited between avalanches after transients have decayed—and the regions leading to avalanches of certain sizes, however, are more complicated. We will outline the derivation of the distribution functions in the following; the detailed, rather tedious calculations can be found in Appendixes A–C. The first step is to obtain a general expression for the volume of region Λ^N, $\mathcal{V}(\Lambda^N(\alpha,U))$, in Π^N. For this purpose, a rule can be derived showing how Λ^N is composed of direct products of *N*-dimensional and lower-dimensional hypercubes of varying side lengths; $\mathcal{V}(\Lambda^N)$ is then given by the sum of the products of the volumes of these hypercubes. As a result, the particularly simple expression $\mathcal{V}(\Lambda^N(\alpha,U))=\alpha U^N$ is obtained for arbitrary *N* (see Appendixes A and B).

For the regions in $\Pi^N(0,U)$ leading to different avalanche sizes, we suppose without loss of generality that the external input ΔU is given to element 1. Upon receiving input, element 1 fires if $u_1>U-\Delta U$. In the second step, the corresponding phase space region, whose volume is given by $U^{N-1}\Delta U$, has to be partitioned into regions where $L-1=0,1,2,\ldots,N-1$ further elements will fire in the respective avalanche. The volumes of these regions will be denoted as $Z(L,N,\alpha)$. The regions and their volumes are constructed iteratively as shown in Appendix C. In the last step, avalanche probabilities $p(L,N,\alpha)$ are obtained by subtracting the volumes of the intersections of the regions $Z(L,N,\alpha)$ with region Λ^N, and subsequently normalizing by the volume of $\Pi^N\backslash\Lambda^N$ (see Appendix C). Using Eq. (3), the avalanche distributions become independent of ΔU and *U*,

$$p(L,N,\alpha)=L^{L-2}\binom{N-1}{L-1}\left(\frac{\alpha}{N}\right)^{L-1}\left(1-L\frac{\alpha}{N}\right)^{N-L-1} \times\frac{N(1-\alpha)}{N-(N-1)\alpha} \quad \text{for} \quad 1\leqslant L\leqslant N. \tag{8}$$

As an example, Figs. 1(a)–1(c) demonstrate the perfect agreement between the analytical result (8) and the numerical avalanche size distributions for $N=10^4$.

Equation (8) resembles the avalanche size distribution which Bröker and Grassberger [[26], Eq. (36)] have found for the random-neighbor OFC model using branching theory. The results differ, in that the result in Ref. [26] yields an expression for avalanche sizes in systems of an arbitrary size *N*, but is valid only in the infinite-size limit where simultaneous avalanches are nonoverlapping. In contrast, Eq. (8) holds for arbitrary system sizes *N* in our model. Formally, Eq. (8) contains a correction factor which is calculated by considering the region Λ^N where the density of states eventually vanishes, instead of assuming a uniform density over the whole configuration space $\Pi^N(0,U)$ divided into regions leading to different avalanche sizes.

3. The thermodynamic limit

Avalanche behavior in the thermodynamic limit $N\to\infty$ can directly be assessed from Eq. (8). Numerical results and

analytical considerations [26] suggest a critical coupling parameter $\alpha_c=1$ for $N\to\infty$. Indeed, an evaluation of Eq. (8) shows that the local exponent

$$\gamma(L)=\lim_{\alpha\to 1}\lim_{N\to\infty}\ln\frac{p(L,N,\alpha)}{p(L+1,N,\alpha)}\Big/\ln\frac{L}{L+1} \tag{9}$$

becomes constant for $L\to\infty$: $\lim_{L\to\infty}\gamma(L)=-3/2$. Thus, in the conservative system, power-law behavior with an exponent of $-3/2$ is reached in the regime of large avalanche sizes. The critical exponent is identical to that of the random-neighbor OFC model [26] and, for example, for mean-field percolation [30].

For finite L, the distribution is actually very close to power-law behavior. Since the critical case corresponds to the conservative system $\alpha=1$, the supracritical regime becomes smaller and smaller as $N\to\infty$: the occurrence of non-monotonic avalanches is a finite-size effect.

4. Avalanche durations

For avalanche durations $p_d(D,N,\alpha)$, an iterative equation for the corresponding regions and their volumes in the configuration space can be derived; cf. Eq. (C23). A closed expression corresponding to the avalanche size distribution (8), however, is not available.

IV. EXTENSIONS AND APPLICATIONS OF THE MODEL IN THE CONTEXT OF NEURAL NETWORKS

Models of SOC can usually be interpreted in terms of neural networks (e.g., Refs. [23,31–34]). Single elements are identified with model neurons that receive both external and internal input. The energy variable corresponds to some internal state of a neuron, usually interpreted as its excitation or membrane potential. Upon reaching a threshold, the neuron is reset and subsequently sends an input to other neurons in the network. In the following, we will study extensions and applications of the avalanche model using neural network terminology.

A. The case $\epsilon<1$

The results described in Sec. III are valid for the Abelian case $\epsilon=1$. In terms of neural networks, this corresponds to a fast neural relaxation such that the excess energy $\tilde{u}_i-U$ is accumulated *after* the reset. For $\epsilon<1$ in Eq. (2), the reset of a neuron is slower, such that a fraction $1-\epsilon$ of the excess energy is lost [34].

We show examples of avalanche size distributions in Fig. 5(a), and examples of duration distributions in Fig. 5(b), for $\epsilon=0.1$.

A conspicuous feature is the appearance of additional peaks also in the regime where avalanches are restricted to sizes $L\leqslant N$. The distributions thus deviate from a power law with a single exponent as in the conservative case $\epsilon=1$. When some neurons cross the threshold, the differences between their membrane potentials before the avalanche, u_i-u_j, will become smaller after the avalanche stopped, $\epsilon(u_i-u_j)$. Therefore $\epsilon<1$ induces peaks in $\rho(u)$, which

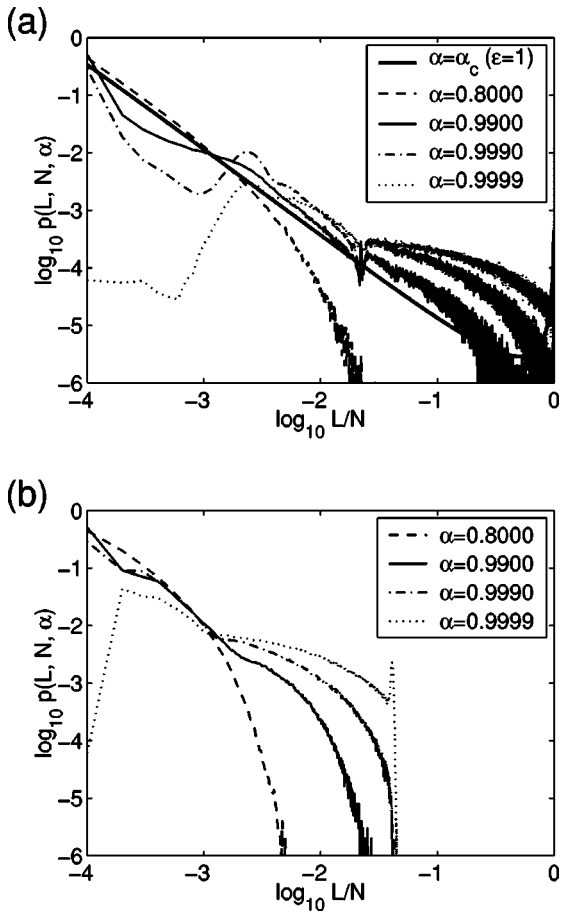

FIG. 5. Distributions of (a) avalanche sizes and (b) avalanche durations for a subcritical coupling strength $\alpha=0.8$ (dashed line) for a critical coupling $\alpha=0.99$ (solid line), a supracritical coupling $\alpha=0.999$ (dashed-dotted line), and a coupling strength of $\alpha=0.9998$ (dotted line). Compare also the distributions shown in Fig. 1 using identical α's. In all cases, the presented curves are temporal averages over 10^6 avalanches with $N=10\,000$, $\Delta U=0.022$, $\epsilon=0.1$, and $U=1$. For comparison, the thick solid line in (a) shows the critical size distribution for $\epsilon=1$.

introduce length scales in the distributions p and p_d, when $\rho(u)$ is rotated in u during an avalanche. The differences between distributions for $\epsilon=1$ and $\epsilon<1$ are most pronounced above $\alpha=\alpha_c$, as can easily be seen in Fig. 5. Small ϵ can also prevent avalanches larger than N in the multi-peaked regime—the dissipation during the reset of the membrane potentials eats up the excess energy which otherwise would make the same neuron fire twice during an avalanche.

Similar avalanche size distributions were described by Corral *et al.* [23] for locally connected networks of integrate-and-fire neurons receiving uniform input to which some noise was added. As in our model, the dissipation of energy was responsible for the occurrence of the peaks whereas in the conservative case, approximate power-law behavior was observed.

B. Avalanches in networks of leaky integrate-and-fire neurons

In the context of biologically motivated neural networks, additional parameters such as time delays of interaction or

decay time constants for the elements' dynamical variable u are usually employed (see, e.g., Refs. [35–41]). Here we briefly show how the avalanche statistics changes by the introduction of a leak term into the dynamical equation (1). Without input to element i, this leak term yields an exponential decay of u_i to zero with time constant τ. For our simulations with leaky threshold neurons, we used a discretized version of the continuous dynamical system

$$\tau \dot{u}_i(t) = -u_i(t) + I_i^{\mathrm{ext}}(t) + I_i^{\mathrm{int}}(t) \quad (i = 1, \ldots, N), \quad (10)$$

with external input $I_i^{\mathrm{ext}}(t) = \delta(t - k\Delta t)\,\delta_{r(k),i}\Delta U$, $k \in \mathbb{Z}$. We define ΔU to be

$$\Delta U = u_0[1 - \exp(-\Delta t/\tau)^N], \quad (11)$$

where $1/\Delta t$ is the rate of the external input and u_0 the asymptotic energy to which an uncoupled neuron would be driven in the absence of a firing threshold. If neuron i reaches its threshold U, the energy is reset to $u_i = 0$.

In the previous, Abelian case we had only one parameter ΔU controlling the input, which had apparently no influence on the shape of the avalanche distributions [see Eq. (8)]. Now, there are two parameters controlling the neuron's input-output characteristics, u_0 and Δt. In the following, we demonstrate the phenomena resulting from varying these input parameters.

In Fig. 6, we choose the critical case $\alpha = \alpha_c$ in a system of $N = 1000$ neurons, while varying u_0. The respective time interval Δt is chosen such that the input ΔU is constant. Effectively, the case $u_0 = \infty$ [Fig. 6(a)] corresponds to neurons without leakage, and decreasing u_0 yields the network behavior for increasing leakage. Such a decrease imposes two changes: first, large avalanches get more and more improbable, and second, oscillations are induced into the size distributions. Both effects can be understood by observing the energy densities $\rho(u)$ (small insets in Fig. 6). While in the nonleaky case [Fig. 6(a)], ρ is nearly uniform, a leaky integration causes more neurons to have energies near the firing threshold U than energies near the resting potential, finally introducing oscillations and peaks in ρ [Figs. 6(b–d)]. These density oscillations lead to the observed oscillations in the size distributions due to the deterministic readout mechanism of the avalanches: during an avalanche, the neural energies are uniformly shifted on the u axis. We observe that the number of oscillatory peaks decreases as u_0 decreases, while the oscillation amplitude increases.

In a second numerical experiment, we held the leakiness constant, while we varied both the rate $1/\Delta t$ at which external input ΔU was delivered, and the coupling constant α such that a transition from subcritical to supracritical occurred. Our results are summarized in Fig. 7. With highly variable external driving, and subcritical coupling (upper left plot in Fig. 7), the neurons do not show any sign of synchronization. When the external driving gets more frequent (lower left plot in Fig. 7), even a small coupling leads to synchronization, accompanied by a strong oscillation. Things do not change significantly when the coupling gets stronger (lower right plot in Fig. 7), only the oscillation period gets shorter and the noise appears to have a stronger influence on the dynamics. When both the variability of the external input and the coupling is high, the system synchronizes *without* oscillating. Here, one element is likely to trigger a large portion of the other elements in the network (synchronization), but the input variability ensures that the membrane potentials of the elements get desynchronized before another avalanche is triggered, preventing an oscillatory component to build up in the cross-correlation functions.

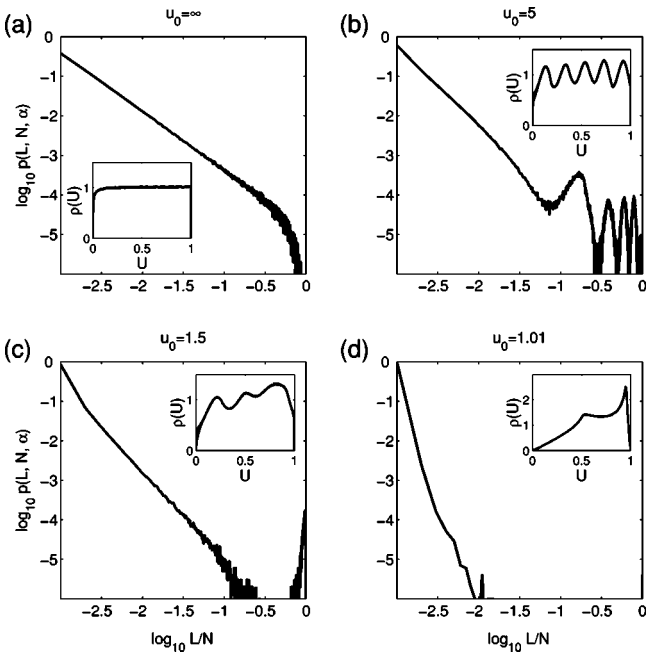

FIG. 6. Distributions of avalanche sizes, $p(L,N,\alpha)$, of a fully connected network of leaky threshold elements receiving random input for different leakiness constants u_0, namely, for (a) $u_0 = \infty$, (b) $u_0 = 5$, (c) $u_0 = 1.5$, and (d) $u_0 = 1.01$. The insets show the corresponding mean energy densities $\rho(u)$. In all cases, the presented curves are temporal averages over 10^6 avalanches with $N = 1000$, $U = 1$, $\Delta U = 0.17$, and $\tau = 1$. With these parameters, the discretization time step Δt was chosen to satisfy Eq. (11).

V. SUMMARY AND CONCLUSION

In summary, we presented an avalanche model involving random input and global coupling between its elements. Avalanche size distributions can be calculated exactly for an arbitrary system size through combinatorial arguments in the system's configuration space. The model therefore accounts for phenomena in finite systems and elucidates the transition to the thermodynamic limit.

The model belongs to the same universality class as the random-neighbor OFC model, showing similar distributions in the subcritical and critical regimes, and the same critical exponent $-3/2$ in the conservative case $\alpha = 1$ as $N \to \infty$.

The analytical access to avalanche size and duration distributions in *finite systems* is especially important when modeling systems that in reality have some 100 to 10 000 elements. For example, cortical columns are examples neural networks with an order of 1000 to 10 000 elements which are

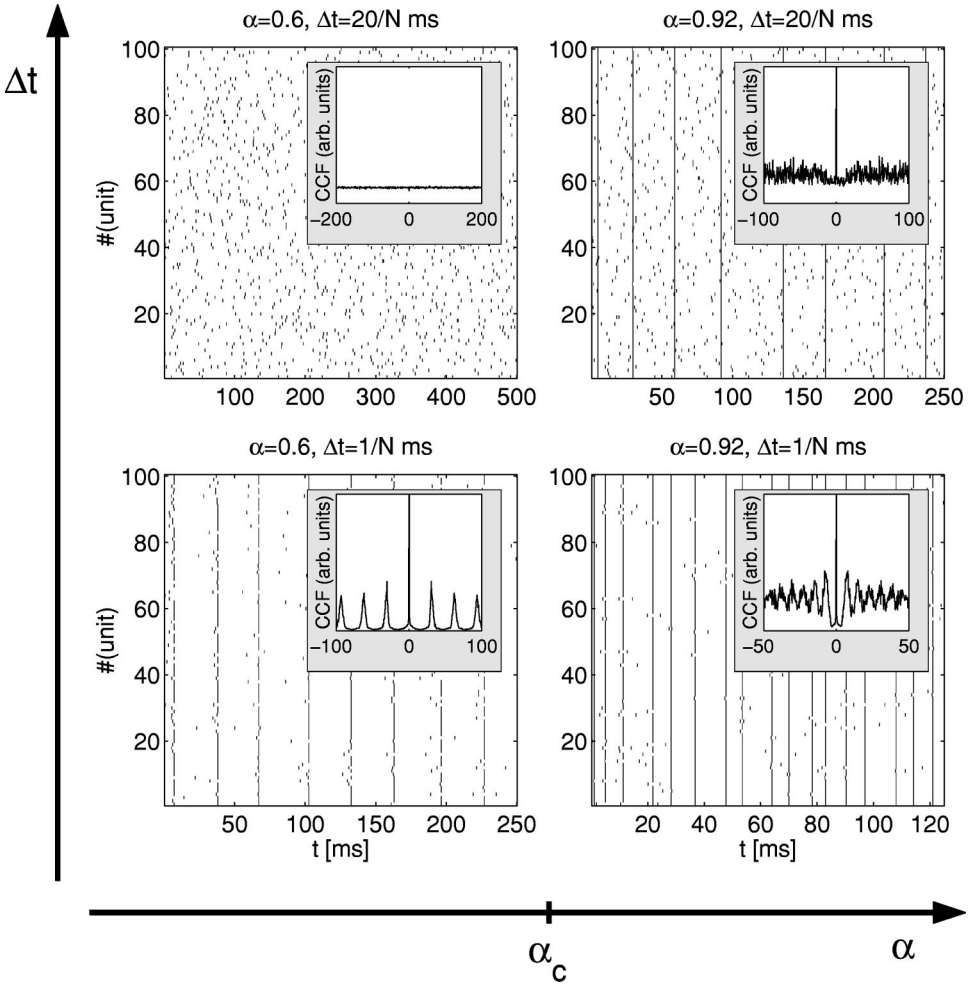

FIG. 7. Raster plots showing the firing dynamics of a network of $N=100$ neurons. Each spike is drawn as a small black tick in dependence of the time t, and the number of the neuron which emitted that spike. The coupling parameter α was chosen to be $\alpha=0.6$ (top left), 0.92 (top right), 0.6 (bottom left), and 0.92 (bottom right), while the time interval between two external inputs was given by $\Delta t=20/N,20/N,1/N$ and $1/N$ m, respectively. The insets show the mean over the cross-correlation functions from 300 pairs selected out of the $N=100$ neurons. The cross-correlation functions have been scaled arbitrarily, but identically for all four insets. u_0 was chosen to be $u_0=1.05$ and $\tau=32.84$ ms, yielding an output rate of 10 Hz for an uncoupled neuron. The critical coupling strength for $N=100$ neurons is $\alpha_{\mathrm{crit}}=0.9$.

densely connected to each other, but sparsely connected to other columns. Our approach may help to understand the synchronization properties of these local networks receiving apparently stochastic input. Even when the analytically solvable Abelian model may abstract from a real neuron, the properties of the avalanche distributions are stable with respect to changes in the underlying model itself—we already pointed out its similarity with the distributions seen in the random-neighbor OFC model. In general, it is not easy to motivate the random-neighbor OFC model, because it employs a coupling changing randomly *in each step* of an avalanche. In the neuronal context, however, the model may be an example of a constantly driven, densely connected network of elements subjected to synaptic failures that occur relatively often in reality.

Among other dynamical properties, we also observe synchronization without oscillations. While this phenomenon has already been observed in biology [42] and modeling studies (see, e.g., Refs. [43,44]), we link its occurrence to the transition from the critical to the supracritical regime. The fact that the latter disappears for large networks goes together with the synchronized dephasing due to finite size first mentioned in Ref. [45] (cf. also Ref. [43]).

With the advance of experimental technologies such as e.g., stable long-time multielectrode recordings, the question of whether one can find similar phenomena in our ''toy'' model as well as in reality arises—our analysis could then provide a tool to understand the mechanisms behind the dynamics. While there are hints that in some cases, power laws can be found in the brain's dynamics [46–48], it remains to elucidate which functional advantage a critical state may have for the information processing going on in the brain.

ACKNOWLEDGMENTS

We would like to thank Professor Theo Geisel for most fruitful discussions at the Max-Planck-Institute for Fluid Dynamics in Göttingen. This work has been supported by the DFG, Sonderforschungsbereich 517 ''Neurokognition'' (U.E. and C.W.E.), and by the Volkswagen Foundation, Project No. 5425 (U.E.).

APPENDIX A: PRELIMINARIES

In the appendixes, we derive the exact avalanche distributions $p(L,N,\alpha)$ for arbitrary system sizes N. Appendix A will introduce a suitable notation for partitioning the configuration space Π into products of lower-dimensional subsets. In Appendix B, we calculate the volume of the region Λ in phase space which is not inhabited between avalanches, by using a partitioning of the configuration space leading to a recursion formula for subregions. In Appendix C, a recur-

sion formula for regions leading to avalanches of a specific size L will be derived, and subsequently be modified by subtracting the noninhabited regions. This modification finally leads to the exact avalanche distributions $p(L,N,\alpha)$.

Before starting the analysis, we will shortly summarize the terminology used in the appendix: $x,y,z\in\mathbb{R}$, and $\boldsymbol{x},\boldsymbol{y},\boldsymbol{z}\in\mathbb{R}^m$; $i,j,k,l,m,n,p,q,r\in\mathbb{N}$ denote indices; I,J,K denote sets of indices. $\mathcal{I},\mathcal{J},\mathcal{K}$ denote second-order sets of indices; $\Pi^m,\Omega^m,\Gamma^m,\Theta^m,\Phi^m\subseteq\mathbb{R}^m$ denote subsets in $\mathbb{R}^m$; D,S,V denote volumes of subsets. Overlined symbols will denote regions and volumes excluding the subset of the non-inhabited volume in configuration space.

1. Subsets and sets of indices

Let $I_{k,m}$ denote an arbitrary k-element subset of $I_m:=\{1,\ldots,m\}$. The superset of all different $I_{k,m}$ is denoted by $\mathcal{I}_{k,m}$. $\mathcal{I}_{k,m}$ contains thus $\binom{m}{k}$ k-element subsets of I_m as its elements.

For the following analysis, it is convenient to define m-dimensional subsets Π^m,

$$\Pi^m(x_{\min},x_{\max}):=\{\boldsymbol{x}\in[x_{\min},x_{\max})^m\subseteq\mathbb{R}^m\}. \tag{A1}$$

The configuration space of N units can then be denoted by $\Pi^N(0,U)$.

We also define subsets $\Gamma_k^m(\lambda,u,I_{k,m})$ for $0<k\leqslant m$ and $0<\lambda\leqslant 1$,

$$\Gamma_k^m(\lambda,u,I_{k,m}):=\left\{\boldsymbol{x}\in\Pi^m(0,u)\,\middle|\,x_i<\lambda\frac{k}{m}u,i\in I_{k,m}\right\}. \tag{A2}$$

Let Λ^m denote a union of Γ_k^m's,

$$\Lambda^m(\lambda,u):=\bigcup_{k=1}^{m}\bigcup_{I_{k,m}\in\mathcal{I}_{k,m}}\Gamma_k^m(\lambda,u,I_{k,m}). \tag{A3}$$

For the special case of $\lambda=1$, $\Gamma_m^m(1,u)=\Pi^m(0,u)$ and, therefore,

$$\Lambda^m(1,u)=\Pi^m(0,u). \tag{A4}$$

In order to be able to combine lower-dimensional subsets, we finally define the direct product $\Theta^k\otimes\Phi^{m-k}|_{I_{k,m}}$ between two subsets. $I_{k,m}$ determines the indices of the components of the elements $\boldsymbol{y}$ in the resulting volume assigned to components belonging to elements $\boldsymbol{x}$ in Θ^k,

$$\Theta^k:=\{\boldsymbol{x}\in A\subseteq\mathbb{R}^k\},$$

$$\Phi^{m-k}:=\{\boldsymbol{x}\in B\subseteq\mathbb{R}^{m-k}\},$$

$$\Theta^k\otimes\Phi^{m-k}|_{I_{k,m}}=\{\boldsymbol{y}\in\mathbb{R}^m|\{y_i\}_{i\in I_{k,m}}\in A,\{y_i\}_{i\in I_m\setminus I_{k,m}}\in B\}. \tag{A5}$$

Note that this definition is well defined only for sets A being invariant under a permutation of the components of $\boldsymbol{x}\in A$. The operator $\otimes$ is assumed to have higher precedence than $\cup,\cap$, and $\setminus$.

2. Lemmas

The following three lemmas will help to shorten the derivation of the recursion formulas in the following sections.

Lemma 1. $\forall k,l\leqslant m;\forall u>0;\forall\lambda:0<\lambda\leqslant 1$,

$$A:=\Pi^l(0,\lambda u)\otimes\Pi^{m-l}(\lambda u,u)|_{J_{l,m}}\cap\Gamma_k^m(\lambda,u,I_{k,m})\neq\varnothing\Leftrightarrow I_{k,m}\subseteq J_{l,m}. \tag{A6}$$

Proof. Let us choose a suitable disjoint decomposition of the index set I_m as

$$\begin{aligned}I_m=&(I_{k,m}\cap J_{l,m})\\&\cup(I_{k,m}\setminus J_{l,m})\\&\cup(J_{l,m}\setminus I_{k,m})\\&\cup(I_m\setminus(I_{k,m}\cup J_{l,m})).\end{aligned} \tag{A7}$$

Using Eqs. (A1), (A3), and (A5), we can then explicitly write A as

$$\begin{aligned}A=\{\boldsymbol{x}\in\mathbb{R}^m|&0\leqslant x_i<\lambda uk/m:i\in I_{k,m}\cap J_{l,m},\\&\lambda u\leqslant x_i<\lambda uk/m:i\in I_{k,m}\setminus J_{l,m},\\&0\leqslant x_i<\lambda u:i\in J_{l,m}\setminus I_{k,m},\\&\lambda u\leqslant x_i<u:i\in I_m\setminus(I_{k,m}\cup J_{l,m})\}.\end{aligned} \tag{A8}$$

Because of $\lambda u\geqslant\lambda uk/m$, A is nonempty if and only if $I_{k,m}\setminus J_{l,m}=\varnothing$; and this implies that $I_{k,m}\subseteq J_{l,m}\Leftrightarrow A\neq\varnothing$. Note that if $k>l$, condition $I_{k,m}\subseteq J_{l,m}$ is never fulfilled.

Lemma 2. $\forall l\leqslant m;\forall u>0;\forall\lambda:0<\lambda\leqslant 1$,

$$\bigcup_{k=1}^{l}\bigcup_{I_{k,m}}\subseteq J_{l,m}\Gamma_k^m(\lambda,u,I_{k,m})=\Lambda^l(\lambda l/m,u)\otimes\Pi^{m-l}(0,u)|_{J_{l,m}}. \tag{A9}$$

Proof. Inserting definition (A2) into the innermost union in Eq. (A9) yields

$$\bigcup_{I_{k,m}\subseteq J_{l,m}}\Gamma_k^m(\lambda,u,I_{k,m})=\bigcup_{I_{k,m}\subseteq J_{l,m}}\left\{\boldsymbol{x}\in\Pi^m(0,u)\,\middle|\,x_j<\lambda\frac{k}{m}u,j\in I_{k,m}\right\}.$$

In this union, exactly $m-l$ components of $\boldsymbol{x}$ cover the whole interval $[0,u)$. By separating these components forming a-

subset $\Pi^{m-l}(0,u)$, the union can be written as a direct product of Π^{m-l} with a union of dimension l, using suitably chosen index sets $K_{k,l}$;

$$\left(\bigcup_{K_{k,l}\in\mathcal{K}_{k,l}} \left\{ \boldsymbol{x}\in\Pi^{l}(0,u) \middle| x_{j\in K_{k,l}} < \lambda \frac{l}{m}\frac{k}{l}u \right\} \right) \otimes \Pi^{m-l}(0,u)\big|_{J_{l,m}} = \left(\bigcup_{K_{k,l}\in\mathcal{K}_{l,k}} \Gamma_k^l(\lambda l/m,u) \right) \otimes \Pi^{m-l}(0,u) \Bigg|_{J_{l,m}} . \tag{A10}$$

Then Eq. (A9) follows immediately, using the definition (A3) for Λ^l.

Lemma 3. $\forall z \leqslant y$,

$$\Lambda^m(x,y)\cap\Pi^m(0,z)=\Lambda^m(xy/z,z). \tag{A11}$$

Proof. This can be achieved by rescaling the parameters u and λ in definition (A2) to the smaller subset $\Pi^m(0,z)$, and inserting the rescaled definition into Eq. (A3).

APPENDIX B: CALCULATION OF THE NONINHABITED VOLUME

In a configuration space of dimension N and volume U^N, the volume not inhabited between avalanches mediated by a coupling of strength $\alpha U/N$ is denoted by $\Lambda^N(\alpha,U)$. The purpose of this section will be to calculate its volume $\mathcal{V}$, which is done iteratively. The reason for using this strategy can be illustrated by comparing the phase spaces and their partitionings for $N=2$ (Fig. 4) and $N=3$ (Fig. 8). The partitioning for $N=2$ is similar to the partitioning of the u_1-u_2 plane in Fig. 8, except for a change in the side lengths of the volumes. This ''self-similiarity'' continues when proceeding to higher N and enables the iterative calculation of the volumes Λ^N. Note that already Λ^3 has a relatively complex structure.

Theorem. $\forall\lambda<u$ and $\forall m>0$, $\mathcal{V}(\Lambda^m(\lambda,u))$ is given by the particularly simple expression

$$\mathcal{V}(\Lambda^m(\lambda,u))=\lambda u^m. \tag{B1}$$

The proof will be given by induction over m.

Basis. From definitions (A3) and (A2) it is obvious that for $m=1$,

$$\mathcal{V}(\Lambda^1(\lambda,u))=\mathcal{V}(\Gamma_1^1(\lambda,u,I_{1,1}))=\lambda u. \tag{B2}$$

Induction. For the induction we assume that Eq. (B2) has been proven for $m=n-1$. Thus we have to prove that Eq. (B2) holds also for $m=n$.

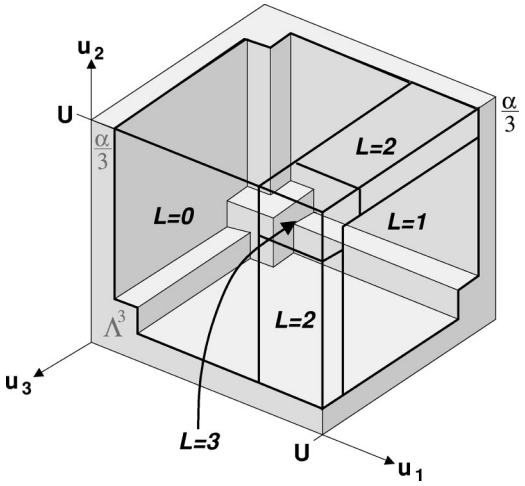

FIG. 8. Example of the configuration space Π^3 and its partitioning. The noninhabited volume Λ^3 is highlighted in shades of gray. The volumes $\overline{V}(L,3,\alpha)$ leading to avalanches of sizes $L=0$, $L=1$, $L=2$, and $L=3$ are outlined with thick black lines at their edges.

The phase space $\Pi^n(0,u)$ can be expressed as a union of disjoint subsets,

$$\Pi^n(0,u)=\bigcup_{l=0}^{n}\bigcup_{J_{l,n}\in\mathcal{I}_{l,n}}\Pi^l(0,\lambda u)\otimes\Pi^{n-l}(\lambda u,u)|_{J_{l,n}}, \tag{B3}$$

whose volumes are related to a binomial expansion of $\mathcal{V}(\Pi^n)$,

$$\mathcal{V}(\Pi^n(0,u))=u^n[\lambda+(1-\lambda)]^n=u^n\sum_{l=0}^{n}\binom{n}{l}\lambda^l(1-\lambda)^{n-l}. \tag{B4}$$

Using the definitions (A1) (A3), it is clear that $\Lambda^n(\lambda,u)\subseteq\Pi^n(0,u)\setminus\Pi^n(\lambda u,u)$. Inserting Eqs. (A3) (B3) into this expression,

$$\Lambda^n(\lambda,u)=[\Pi^n(0,u)\setminus\Pi^n(\lambda u,u)]\cap\Lambda^n(\lambda,u) = \left(\bigcup_{l=1}^{n}\bigcup_{J_{l,n}\in\mathcal{I}_{l,n}}\Pi^l(0,\lambda u)\otimes\Pi^{n-l}(\lambda u,u)|_{J_{l,n}}\right) \cap\left(\bigcup_{k=1}^{n}\bigcup_{I_{k,n}\in\mathcal{I}_{k,n}}\Gamma_k^n(\lambda,u,I_{k,n})\right).$$

We subsequently use Lemmas (A6), (A9), and (A11) and obtain

$$\bigcup_{l=1}^{n}\bigcup_{\substack{J_{l,n}\\ \in\mathcal{I}_{l,n}}}\left(\Pi^{l}(0,\lambda u)\otimes\Pi^{n-l}(\lambda u,u)\big|_{J_{l,n}}\cap\bigcup_{k=1}^{l}\bigcup_{I_{k,n}\subseteq J_{l,n}}\Gamma_{k}^{n}(\lambda,u,I_{k,n})\right)\quad[\text{Eq. (A6)}]$$

$$=\bigcup_{l=1}^{n}\bigcup_{\substack{J_{l,n}\\ \in\mathcal{I}_{l,n}}}\left(\Pi^{l}(0,\lambda u)\otimes\Pi^{n-l}(\lambda u,u)\big|_{J_{l,n}}\cap\Lambda^{l}(\lambda l/n,u)\otimes\Pi^{n-l}(0,u)\big|_{J_{l,n}}\right)\quad[\text{Eq. (A9)}]$$

$$=\bigcup_{l=1}^{n}\bigcup_{J_{l,n}\in\mathcal{I}_{l,n}}(\Pi^{l}(0,\lambda u)\cap\Lambda^{l}(\lambda l/n,u))\otimes(\Pi^{n-l}(\lambda u,u)\cap\Pi^{n-l}(0,u))\big|_{J_{l,n}},$$

$$=\bigcup_{l=1}^{n}\bigcup_{\substack{J_{l,n}\\ \in\mathcal{I}_{l,n}}}\Lambda^{l}\left(\frac{l}{n},\lambda u\right)\otimes\Pi^{n-l}(\lambda u,u)\Big|_{J_{l,n}}\quad[\text{Eq. (A11)}].\tag{B5}$$

By construction [see Eq. (B3)], the subsets are disjoint and the volume $\mathcal{V}$ of their union can be written as a sum over the subvolumes. In addition, volumes of subsets for different index sets $J_{l,n}$ for fixed n and l are identical. Thus we can insert Eq. (B1) for $l<n$, and Eq. (A4) for $l=n$. Through this procedure we close the induction

$$\mathcal{V}(\Lambda^{n}(\lambda,u))=\sum_{l=1}^{n}\binom{n}{l}\frac{l}{n}(\lambda u)^{l}u^{n-l}(1-\lambda)^{n-l}$$

$$=\lambda u^{n}\sum_{l=1}^{n}\binom{n-1}{l-1}\lambda^{l-1}(1-\lambda)^{n-l}$$

$$=\lambda u^{n}\sum_{k=0}^{n-1}\binom{n-1}{k}\lambda^{k}(1-\lambda)^{(n-1)-k}=\lambda u^{n}.\quad\blacksquare\tag{B6}$$

By choosing $n=N$, $u=U$, and $\lambda=\alpha$, we obtain the volume $\mathcal{V}$ for the noninhabited region as

$$\mathcal{V}(\Lambda^{N}(\alpha,U))=\alpha U^{N}.\tag{B7}$$

APPENDIX C: AVALANCHE DISTRIBUTIONS

In this section, we will prove the following theorem for the avalanche probabilities $p(L,N,\alpha)$.

Theorem.

$$p(L,N,\alpha)=L^{L-2}\binom{N-1}{L-1}\left(\frac{\alpha}{N}\right)^{L-1}\times\left(1-L\frac{\alpha}{N}\right)^{N-L-1}\frac{N(1-\alpha)}{N-(N-1)\alpha}.\tag{C1}$$

Proof. It is convenient to divide the proof into three steps. The first step will be to identify the regions in configuration space leading to avalanches of a certain size L. The second step will be to subtract the noninhabited subset Λ^{N} from these regions. By calculating their volume, one finally obtains the correct avalanche probabilities $p(L,N,\alpha)$. As in the preceding appendix, we will use an iterative procedure, as suggested by comparing Figs. 4 and 8.

1. Regions representing different avalanche sizes

To convey the idea behind the analysis, we first recall the dynamics during one event in an avalanche. Typically, m units have still not been active yet, l units are just firing, k elements have already fired and will not be activated again, and j of the m remaining units will be activated until the avalanche stops. If the coupling strength is $\beta=\alpha U/N$, no state variable u of the remaining m units could have been initially larger than $U-k\beta$. We will denote the m-dimensional subsets of the configuration space, which will evolve into the situation described above, with $\Omega_{k,l}^{m}(j)$. The following considerations will lead to a recursion formula for $\Omega_{k,l}^{m}(j)$ over the variable j.

Let us start with the subspace $\Pi^{m}(0,U-k\beta)$, which can be written as a union over all Ω's with fixed k, l, and m,

$$\Pi^{m}(0,U-k\beta)=\bigcup_{j=0}^{m}\Omega_{k,l}^{m}(j).\tag{C2}$$

In other words, Eq. (C2) expresses that an m-dimensional configuration space of side length $U-k\beta$, onto which an input of $l\beta$ is given, can be decomposed into subsets where j units will fire. It is obvious that for the case $j=0$ in which an avalanche stops, the subset $\Omega_{k,l}^{m}(0)$ is given by

$$\Omega_{k,l}^{m}(0)=\Pi^{m}(0,U-(k+l)\beta).\tag{C3}$$

While decomposition (C2) partitions Π^{m} considering the whole remaining part of an avalanche with j units firing, one can equally well partition Π^{m} considering only the next step in an avalanche, where the input of $l\beta$ can trigger up to m units to fire immediately. With i denoting the number of these units, the disjoint decomposition then reads

$$\Pi^m(0,U-k\beta)=\bigcup_{i=0}^{m}\bigcup_{I_{i,m}\in\mathcal{I}_{i,m}}\Pi^{m-i}(0,U-(k+l)\beta)\otimes\Pi^i(U-(k+l)\beta,U-k\beta)\Big|_{I_{m-i,m}}. \tag{C4}$$

Using an appropriately scaled (C2) as a decomposition of Π^{m-i}, the common input $i\beta$ due to the i units firing will subsequently trigger $j'-i$ elements until the avalanche stops,

$$\Pi^{m-i}(0,U-(k+l)\beta)=\bigcup_{j'=i}^{m}\Omega^{m-i}_{k+l,i}(j'-i). \tag{C5}$$

Inserting Eq. (C5) into Eq. (C4), and comparing Eqs. (C2) (C4), one obtains after changing the precedence of the unions over i and j',

$$\begin{aligned}\bigcup_{j=1}^{m}\Omega^m_{k,l}(j)&=\bigcup_{i=1}^{m}\bigcup_{I_{i,m}\in\mathcal{I}_{i,m}}\left(\bigcup_{j'=i}^{m}\Omega^{m-i}_{k+l,i}(j'-i)\right)\otimes\Pi^i(U-(k+l)\beta,U-k\beta)\Big|_{I_{m-i,m}}\\&=\bigcup_{j'=1}^{m}\bigcup_{i=1}^{j'}\bigcup_{I_{i,m}\in\mathcal{I}_{i,m}}\Omega^{m-i}_{k+l,i}(j'-i)\otimes\Pi^i(U-(k+l)\beta,U-k\beta)\Big|_{I_{m-i,m}}.\end{aligned} \tag{C6}$$

In Eq. (C6), we excluded subsets where the input $l\beta$ triggers none of the units, because we already know the result from Eq. (C3).

If we require Eq. (C6) to represent a recursive description of the avalanche dynamics, then one specific $\Omega^m_{k,l}(j)$ should be composed of terms with j' satisfying $(j'-i)+i=j$,

$$\Omega^m_{k,l}(j)=\bigcup_{i=1}^{j}\bigcup I_{i,m\in\mathcal{I}_{i,m}}\Omega^{m-i}_{k+l,i}(j-i)\otimes\Pi^i(U-(k+l)\otimes\beta,U-k\beta)\big|_{I_{m-i,m}}. \tag{C7}$$

This expression is the required recursion formula.

2. Subtraction of the noninhabited region

For the following considerations, we introduce the abbreviation $\Phi^n:=\Pi^n(U-(k+l)\beta,U-k\beta)$.

We define $\overline{\Omega}$ by subtracting Λ^N from Ω,

$$\overline{\Omega}^m_{k,l}(j)\otimes\Phi^{N-m}\big|_{I_{m,N}}:=\Omega^m_{k,l}(j)\otimes\Phi^{N-m}\big|_{I_{m,N}}\setminus\Lambda^N(\alpha,U). \tag{C8}$$

If $k+l\leqslant N$, using Eqs. (A2) and (A3) reveals that $\Phi^n\cap\Lambda^N(\alpha,U)=\varnothing$. Through this property, Eq. (C7) remains valid if one replaces the Ω's by the $\overline{\Omega}$'s.

Thus it suffices to explicitly compute $\overline{\Omega}^m_{k,l}(j)$ for $j=0$. Inserting Eq. (A3) into Eq. (C8), and using Lemmas (A6), (A9), and (A11) yields

$$\begin{aligned}&\overline{\Omega}^m_{k,l}(0)\otimes\Phi^{N-m}\big|_{I_{m,N}}\\&\quad=\Omega^m_{k,l}(0)\otimes\Phi^{N-m}\big|_{I_{m,N}}\setminus\bigcup_{i=1}^{m}\bigcup_{J_{i,N}\subseteq I_{m,N}}\Gamma^N_i(\alpha,U,J_{i,N})\quad[\text{Eq. (A6)}]\\&\quad=\Omega^m_{k,l}(0)\otimes\Phi^{N-m}\big|_{I_{m,N}}\setminus\Lambda^m(\alpha m/N,U)\otimes\Pi^{N-m}(0,U)\big|_{I_{m,N}}\quad[\text{Eq. (A9)}]\\&\quad=\left[\Omega^m_{k,l}(0)\setminus\Lambda^m\left(\frac{m\alpha U/N}{U-(k+l)\beta},U-(k+l)\beta\right)\right]\otimes\Phi^{N-m}\big|_{I_{m,N}}\quad[\text{Eq. (A11)}].\end{aligned} \tag{C9}$$

From this expression, $\overline{\Omega}^m_{k,l}(0)$ can be extracted as

$$\overline{\Omega}^m_{k,l}(0)=\Omega^m_{k,l}(0)\setminus\Lambda^m\left(\frac{m\alpha U/N}{U-(k+l)\beta},U-(k+l)\beta\right). \tag{C10}$$

3. Calculation of the volumes of the regions

With $S^m_{k,l}(j):=\mathcal{V}(\Omega^m_{k,l}(j))$ and $\overline{S}^m_{k,l}(j):=\mathcal{V}(\overline{\Omega}^m_{k,l}(j))$, Eqs. (C3) and (C7) define recursions for configuration space volumes

$$S_{k,l}^{m}(j)=\begin{cases}(U-(k+l)\beta)^{m}, & j=0\\ \sum_{i=1}^{j}\binom{m}{i}(l\beta)^{i}S_{k+l,i}^{m-i}(j-i), & j\leqslant m,\end{cases} \quad \text{(C11)}$$

$$\overline{S}_{k,l}^{m}(j)=\begin{cases}(U-(k+l)\beta)^{m-1}(U-(k+l+m)\beta), & j=0\\ \sum_{i=1}^{j}\binom{m}{i}(l\beta)^{i}\overline{S}_{k+l,i}^{m-i}(j-i), & j\leqslant m,\end{cases} \quad \text{(C12)}$$

where $\overline{S}_{k,l}^{m}(0)$ was possible to calculate from $S_{k,l}^{m}(0)$ by simply subtracting the volume of Λ^{m}, because its size in Eq. (C10) has been scaled not to extend over $\Omega_{k,l}^{m}(0)$,

$$\overline{S}_{k,l}^{m}(0)=S_{k,l}^{m}(0)-\alpha U\frac{m}{N}(U-(k+l)\beta)^{m-1}. \quad \text{(C13)}$$

Using similar arguments, one also obtains a recursion for the volumes $D_{k,l}^{m}(j)$ corresponding to regions of avalanche durations j,

$$D_{k,l}^{m}(j)=\sum_{i=1}^{m-j+1}\binom{m}{i}(l\beta)^{i}D_{k+l,i}^{m-i}(j-1), \quad \text{(C14)}$$

for $0<j\leqslant N$ and $D_{k,l}^{m}(0)=S_{k,l}^{m}(0)$. Correcting for the noninhabited volume leads to the same recursion for the volumes $\overline{D}_{k,l}^{m}(j)$ for $0<j\leqslant N$ with $\overline{D}_{k,l}^{m}(0)=\overline{S}_{k,l}^{m}(0)$.

To obtain a closed expression for the volumes S and $\overline{S}$, we will now prove the following proposition.

Proposition. For $U>0, k+l+j<N$, and $j\leqslant m$,

$$S_{k,l}^{m}(j)=\binom{m}{j}\beta^{j}l(j+l)^{j-1}(U-(k+l+j)\beta)^{m-j},$$

$$\overline{S}_{k,l}^{m}(j)=\binom{m}{j}\beta^{j}l(j+l)^{j-1}(U-(k+l+j)\beta)^{m-j-1}\times(U-(m+k+l)\beta). \quad \text{(C15)}$$

The proof is possible by induction over n, and it is very similar for S and $\overline{S}$. We will therefore only give the proof for $\overline{S}$ in order to shorten this appendix.

Basis. For $m=1$, j can either be 0 or 1, and using Eq. (C13) leads to

$$\overline{S}_{k,l}^{1}(0)=(U-(1+k+l)\beta)^{1}, \quad \text{(C16)}$$

$$\overline{S}_{k,l}^{1}(1)=(l\beta)^{1}. \quad \text{(C17)}$$

Induction. For the induction we assume that Eq. (C15) has been proven for $m\leqslant n-1$. Thus we have to prove that Eq. (C15) holds also for $m=n$,

$$\begin{aligned}\overline{S}_{k,l}^{m}(j)&=\sum_{i=1}^{j}\binom{m}{i}(l\beta)^{i}\overline{S}_{k+l,i}^{m-i}(j-i)\\ &=\sum_{i=1}^{j}\binom{m}{i}(l\beta)^{i}\binom{m-i}{j-i}\beta^{j-i}(U-(m+k+l)\beta)(U-(k+l+j)\beta)^{m-j-1}i(j-i+i)^{j-i-1}\\ &=\binom{m}{j}\beta^{j}(U-(k+l+j)\beta)^{m-j-1}(U-(m+k+l)\beta)\left\{\sum_{i=1}^{j}l^{i}\binom{j}{i}ij^{j-i-1}\right\}\\ &=\binom{m}{j}\beta^{j}(U-(k+l+j)\beta)^{m-j-1}(U-(m+k+l)\beta)\left\{l\sum_{i'=0}^{j-1}\binom{j-1}{i'}l^{i'}j^{(j-1)-i'}\right\}\\ &=\binom{m}{j}\beta^{j}l(l+j)^{r-1}(U-(k+l+j)\beta)^{m-j-1}(U-(m+k+l)\beta). \quad \blacksquare\end{aligned} \quad \text{(C18)}$$

With this closed expression, it will be possible to finally calculate an expression of the avalanche probabilities.

4. Avalanche probabilities

An avalanche starts if one unit is triggered by an input of strength ΔU to fire. Thus the phase space volumes $\overline{V}(L,N,\alpha)$ and $V(L,N,\alpha)$ for avalanches of size $L>0$ are obtained by multiplying ΔU with $\overline{S}_{0,1}^{N-1}(L-1)$ and $S_{0,1}^{N-1}(L-1)$, respectively. These specific S's are the volumes of the subsets of dimension $N-1$ containing states for which $j=L-1$ neurons will subsequently fire, triggered by an input of $l\beta$ with $l=1$. $\overline{V}(0,N,\alpha)$ and $V(0,N,\alpha)$ can be computedas the remaining part of the whole phase space, and we obtain

$$V(L,N,\alpha)=\begin{cases} U^{N-1}(U-\Delta U), & L=0 \\ \Delta U S_{0,1}^{N-1}(L-1), & L>0, \end{cases}$$

$$=\begin{cases} U^{N-1}(U-\Delta U), & L=0 \\ \dfrac{\Delta U}{L}U^{N-1}\binom{N-1}{L-1}\left(\dfrac{L\alpha}{N}\right)^{L-1}\left(1-\dfrac{L\alpha}{N}\right)^{N-L}, & L>0 \end{cases} \tag{C19}$$

and

$$\overline{V}(L,N,\alpha)=\begin{cases} U^{N-1}(1-\alpha)\left[U-\Delta U\left(1-\alpha-\dfrac{\alpha}{N}\right)\right], & L=0 \\ \dfrac{\Delta U}{L}U^{N-1}\binom{N-1}{L-1}\left(\dfrac{L\alpha}{N}\right)^{L-1}\left(1-\dfrac{L\alpha}{N}\right)^{N-L-1}(1-\alpha), & L>0. \end{cases} \tag{C20}$$

The probability of an avalanche $P(L,N,\alpha)$ is then given by $P(L,N,\alpha)=\overline{V}(L,N,\alpha)/\mathcal{V}(\Pi^N(0,\alpha)\setminus\Lambda^N(0,\alpha))$. With Eq. (B1), $\mathcal{V}(\Pi^N(0,\alpha)\setminus\Lambda^N(0,\alpha))=U^N(1-\alpha)$; then using Eq. (3) leads to the final result [see also Eq. (8)]

$$p(L,N,\alpha)=\frac{\overline{V}(L,N,\alpha)}{U^N(1-\alpha)-\overline{V}(0,N,\alpha)}=\frac{1}{L}\binom{N-1}{L-1}\times\left(L\frac{\alpha}{N}\right)^{L-1}\left(1-L\frac{\alpha}{N}\right)^{N-L-1}\frac{N(1-\alpha)}{N-(N-1)\alpha}. \quad \blacksquare \tag{C21}$$

If $p(L,N,\alpha)$ had been calculated without subtracting the noninhabited region, the final expression would have read [50]

$$p(L,N,\alpha)=\frac{1}{L}\binom{N-1}{L-1}\left(L\frac{\alpha}{N}\right)^{L-1}\left(1-L\frac{\alpha}{N}\right)^{N-L}. \tag{C22}$$

With similar arguments, the expression for the avalanche durations $p_d(L,N,\alpha)$ becomes

$$p_d(L,N,\alpha)=\frac{\Delta U\overline{D}_{0,1}^{N-1}(L-1)}{U^N(1-\alpha)\left[1-U+\Delta U\left(1-\alpha-\dfrac{\alpha}{N}\right)\right]}. \tag{C23}$$

[1] V. Frette, K. Christensen, A.M. Malthe-Sørenssen, J. Feder, T. Jøssang, and P. Meakin, Nature (London) **397**, 49 (1996).
[2] B. Gutenberg and C.F. Richter, Ann. Geophys. (C.N.R.S.) **9**, 1 (1956).
[3] P. Bak, K. Chen, and M. Creutz, Nature (London) **342**, 780 (1989).
[4] H.J.S. Feder and J. Feder, Phys. Rev. Lett. **66**, 2669 (1991).
[5] A.M. Alencar, S.V. Buldyrev, A. Majumdar, H.E. Stanley, and B. Suki, Phys. Rev. Lett. **87**, 088101 (2001).
[6] P. Bak, C. Tang, and K. Wiesenfeld, Phys. Rev. Lett. **59**, 381 (1987).
[7] P. Bak, C. Tang, and K. Wiesenfeld, Phys. Rev. A **38**, 364 (1988).
[8] L.P. Kadanoff, S.R. Nagel, L. Wu, and S. Zhou, Phys. Rev. A **39**, 6524 (1989).
[9] G. Grinstein, D.-H. Lee, and S. Sachdev, Phys. Rev. Lett. **64**, 1927 (1990).
[10] L. Pietronero, A. Vespignani, and S. Zapperi, Phys. Rev. Lett. **72**, 1690 (1994).
[11] D. Sornette, A. Johansen, and I. Dornic, J. Phys. I **5**, 325 (1995).
[12] A. Vespignani, S. Zapperi, and V. Loreto, Phys. Rev. Lett. **77**, 4560 (1996).
[13] A. Vespignani and S. Zapperi, Phys. Rev. Lett. **78**, 4793 (1997).
[14] D. Dhar and R. Ramaswamy, Phys. Rev. Lett. **63**, 1659 (1989).
[15] D. Dhar, Phys. Rev. Lett. **64**, 1613 (1990).
[16] T. Hwa and M. Kardar, Phys. Rev. Lett. **62**, 1813 (1989).
[17] S.S. Manna, L.B. Kiss, and J. Kertész, J. Stat. Phys. **61**, 923 (1990).
[18] T. Tsuchiya and M. Katori, Phys. Rev. E **61**, 1183 (2000).
[19] Z. Olami, H.J.S. Feder, and K. Christensen, Phys. Rev. Lett. **68**, 1244 (1992).
[20] K. Christensen and Z. Olami, Phys. Rev. A **46**, 1829 (1992).
[21] J.E.S. Socolar, G. Grinstein, and C. Jayaprakash, Phys. Rev. E **47**, 2366 (1993).
[22] P. Grassberger, Phys. Rev. E **49**, 2436 (1994).
[23] Á. Corral, C.J. Pérez, A. Díaz-Guilera, and A. Arenas, Phys. Rev. Lett. **74**, 118 (1995).
[24] A.A. Middleton and C. Tang, Phys. Rev. Lett. **74**, 742 (1995).
[25] S. Lise and H.J. Jensen, Phys. Rev. Lett. **76**, 2326 (1996).
[26] H.-M. Bröker and P. Grassberger, Phys. Rev. E **56**, 3944 (1997).
[27] M.-L. Chabanol and V. Hakim, Phys. Rev. E **56**, R2343 (1997).
[28] O. Kinouchi, S.T.R. Pinho, and C.P.C. Prado, Phys. Rev. E **58**, 3997 (1998).

[29] H.-M. Bröker and P. Grassberger, Europhys. Lett. **30**, 319 (1995).
[30] D. Stauffer, *Introduction to Percolation Theory* (Taylor & Francis, London, 1985).
[31] A. Corral, C.J. Pérez, A. Díaz-Guilera, and A. Arenas, Phys. Rev. Lett. **75**, 3697 (1995).
[32] M. Usher, M. Stemmler, and Z. Olami, Phys. Rev. Lett. **74**, 326 (1995).
[33] S. Bottani, Phys. Rev. Lett. **74**, 4189 (1995).
[34] A.V.M. Herz and J.J. Hopfield, Phys. Rev. Lett. **75**, 1222 (1995).
[35] U. Ernst, K. Pawelzik, and T. Geisel, Phys. Rev. Lett. **74**, 1570 (1995).
[36] J.J. Hopfield, Nature (London) **376**, 33 (1995).
[37] J.J. Hopfield and A.V.M. Herz, Proc. Natl. Acad. Sci. U.S.A. **92**, 6655 (1995).
[38] W. Gerstner, Phys. Rev. Lett. **76**, 1755 (1996).
[39] J. Foss, F. Moss, and J.G. Milton, Phys. Rev. E **55**, 4536 (1997).
[40] B. Ruf and M. Schmitt, IEEE Trans. Neural Netw. **9**, 575 (1998).
[41] C.W. Eurich, K. Pawelzik, U. Ernst, J.D. Cowan, and J.G. Milton, Phys. Rev. Lett. **82**, 1594 (1999).
[42] W.A. Phillips and W. Singer, Behav. Brain Sci. **20**, 657 (1997).
[43] C. Koch and H. Schuster, Neural Comput. **4**, 211 (1992).
[44] J. Lin, K. Pawelzik, U. Ernst, and T. Sejnowski, Network **9**, 333 (1998).
[45] H. Sompolinsky, D. Golomb, and D. Kleinfeld, Proc. Natl. Acad. Sci. U.S.A. **87**, 7200 (1990).
[46] M.C. Teich, IEEE Trans. Biomed. Eng. **36**, 150 (1989).
[47] F. Grüneis, M. Nakao, M. Yamamoto, T. Musha, and H. Nakahama, Biol. Cybern. **60**, 161 (1989).
[48] F. Grüneis, M. Nakao, and M. Yamamoto, Biol. Cybern. **62**, 407 (1990).
[49] The term ''critical'' is applied to finite systems here meaning an approximate power-law behavior; true criticality requires the thermodynamic limit $N\rightarrow\infty$, which will be discussed below.
[50] By mapping the variable names $L\mapsto s$, $L\alpha/N\mapsto p$, and $(N-1)/L\mapsto n$, expression (C22) becomes identical to Eq. (36) in Ref. [26].